Structure in the COBE differential microwave radiometer first-year maps

Article *in* The Astrophysical Journal · September 1992

DOI: 10.1086/186504 · Source: NTRS

28 authors, including:

George Smoot
The Hong Kong University of Science and Technology
645 PUBLICATIONS **36,465** CITATIONS
SEE PROFILE

Giovanni de Amici
NASA
83 PUBLICATIONS **4,713** CITATIONS
SEE PROFILE

Samuel Gulkis
JPL, California Institute of Technology, Pasadena, CA
332 PUBLICATIONS **9,051** CITATIONS
SEE PROFILE

M. G. Hauser
Space Telescope Science Institute
147 PUBLICATIONS **11,948** CITATIONS
SEE PROFILE

THE ASTROPHYSICAL JOURNAL, 396:L1–L5, 1992 September 1

STRUCTURE IN THE *COBE*[1] DIFFERENTIAL MICROWAVE RADIOMETER FIRST-YEAR MAPS

G. F. SMOOT,[2] C. L. BENNETT,[3] A. KOGUT,[4] E. L. WRIGHT,[5] J. AYMON,[2] N. W. BOGGESS,[3] E. S. CHENG,[3]
G. DE AMICI,[2] S. GULKIS,[6] M. G. HAUSER,[3] G. HINSHAW,[4] P. D. JACKSON,[7] M. JANSSEN,[6]
E. KAITA,[7] T. KELSALL,[3] P. KEEGSTRA,[7] C. LINEWEAVER,[2] K. LOEWENSTEIN,[7] P. LUBIN,[8]
J. MATHER,[3] S. S. MEYER,[9] S. H. MOSELEY,[3] T. MURDOCK,[10] L. ROKKE,[7]
R. F. SILVERBERG,[3] L. TENORIO,[2] R. WEISS,[9] AND D. T. WILKINSON[11]
Received 1992 April 21; accepted 1992 June 12

ABSTRACT

The first year of data from the Differential Microwave Radiometers (DMR) on the *Cosmic Backgoround Explorer* (*COBE*) show statistically significant ($>7\ \sigma$) structure that is well described as scale-invariant fluctuations with a Gaussian distribution. The major portion of the observed structure cannot be attributed to known systematic errors in the instrument, artifacts generated in the data processing, or known Galactic emission. The structure is consistent with a thermal spectrum at 31, 53, and 90 GHz as expected for cosmic microwave background anisotropy.

The rms sky variation, smoothed to a total 10° FWHM Gaussian, is $30 \pm 5\ \mu$K ($\Delta T/T = 11 \times 10^{-6}$) for Galactic latitude $|b| > 20°$ data with the dipole anisotropy removed. The rms cosmic quadrupole amplitude is $13 \pm 4\ \mu$K ($\Delta T/T \approx 5 \times 10^{-6}$). The angular autocorrelation of the signal in each radiometer channel and cross-correlation between channels are consistent and give a primordial fluctuation power-law spectrum with index $n = 1.1 \pm 0.5$, and an rms-quadrupole–normalized amplitude of $16 \pm 4\ \mu$K ($\Delta T/T \approx 6 \times 10^{-6}$). These features are in accord with the Harrison-Zel'dovich (scale-invariant, $n = 1$) spectrum predicted by models of inflationary cosmology. The low overall fluctuation amplitude is consistent with theoretical predictions of the minimal level gravitational potential variations that would give rise to the observed present day structure.

Subject headings: cosmic microwave background — cosmology: observations

1. INTRODUCTION

The 2.73 K cosmic microwave background (CMB) is one of the most effective probes of the early universe. On large angular scales the CMB contains imprints of the primordial gravitational potential fluctuations (Sachs & Wolfe 1967) thought to be the origin of large-scale structure in the universe. The *COBE* DMR instrument, described by Smoot et al. (1990), is designed to measure the large-angular–scale anisotropy of the CMB. The instrument operates at three frequencies: 31.5, 53, and 90 GHz (wavelengths 9.5, 5.7, and 3.3 mm), chosen to be near the minimum in Galactic emission and near the CMB maximum. There are two nearly independent channels, A and B, at each frequency. The orbit and pointing of *COBE* result in a complete survey of the sky every 6 months while shielding the DMR from terrestrial and solar radiation (Boggess et al. 1992). Smoot et al. (1991) present preliminary results based on 6 months of data and Bennett et al. (1992a) describe the calibration procedures. This *Letter* describes results based upon the first year of DMR data. Companion papers discuss the treatment of systematic errors (Kogut et al. 1992), discuss the separation of cosmic and Galactic signals (Bennett et al. 1992b), and compare these data to other measurements and to models of structure formation through gravitational instability (Wright et al. 1992). These new results are consistent with, and substantially more sensitive than, the previously published large-angular–scale anisotropy measurements, in particular those of Princeton (Fixsen et al. 1983), Berkeley (Lubin et al. 1985), Relikt (Klypin et al. 1987), DMR preliminary results (Smoot et al. 1991), and Meyer, Page, & Cheng (1991).

2. DATA PROCESSING AND ANALYSIS

The DMR measures the difference in antenna temperature between regions of the sky separated by 60°. A baseline is subtracted for each radiometer channel and the data are converted from telemetry units to antenna temperature. We reject data taken when the Earth is 1° below the Sun/Earth shield or higher (5.0% of data), when the Moon is within 25° of an antenna beam center (6.6% of data), when any datum deviates from the daily mean by more than $5\ \sigma$ ($<0.001\%$ of data), or when the spacecraft telemetry or attitude solution is of poor quality (1.5% of data). The remaining data are corrected for emission from the Moon and Jupiter, the Doppler effect of the spacecraft velocity about the Earth and the Earth motion about the solar system barycenter, and the instrument susceptibility to the Earth's magnetic field. A least-squares mini-

[1] The National Aeronautics and Space Administration/Goddard Space Flight Center (NASA/GSFC) is responsible for the design, development, and operation of the *Cosmic Background Explorer* (*COBE*), Scientific guidance is provided by the *COBE* Science Working Group. GSFC is also responsible for the development of the analysis software and for the production of the mission data sets.

[2] Lawrence Berkeley Laboratory, Space Sciences Laboratory, and Center for Particle Astrophysics, Building 50-351, University of California, Berkeley, CA 94720.
[3] NASA Goddard Space Flight Center, Code 685, Greenbelt, MD 20771.
[4] University Space Research Association, Code 610.3, NASA/GSFC, Greenbelt, MD 20771.
[5] University of California at Los Angeles, Astronomy Department, Los Angeles, CA 90024-1562.
[6] Jet Propulsion Laboratory, Pasadena, CA 91109.
[7] Hughes STX Corporation, 4400 Forbes Boulevard, Lanham, MD 20706.
[8] University of California at Santa Barbara, Physics Department, Santa Barbara, CA 93106.
[9] Massachusetts Institute of Technology, Department of Physics, Room 20F-001, Cambridge, MA 02139.
[10] General Research Corporation, 5 Cherry Hill Drive, Danvers, MA 01923.
[11] Princeton University, Department of Physics, Princeton, NJ 08540.

mization is used to fit the data to spherical harmonic expansions and to make sky maps with 6144 nearly equal area pixels using a sparse matrix technique (Torres et al. 1989; Janssen & Gulkis 1992).

We have searched the DMR time-ordered data and maps for evidence of systematic artifacts (Kogut et al. 1992). The largest such effect is the instrument response to an external magnetic field, which is modeled as a linear function of the Earth's field and the radiometer orientation. A least-squares minimization is used to fit simultaneously the sky temperature distribution and the instrument magnetic response. The magnetic corrections are on the scale of 10–100 μK in the time-ordered data. Residual errors in the individual radiometer channel maps, after correction, are typically 2 μK and never more than 8.5 μK.

Data binned by the position of the Earth relative to the spacecraft show no evidence for Earth emission at the noise limit (47 μK at 95% CL). The estimated Earth emission in the maps is less than 2 μK. The time-ordered data with antenna beam centers more than 25° away from the Moon are corrected to an estimated accuracy of 10% (4 μK). The estimated residual effect on the maps is less than 1 μK.

Kogut et al. list upper limits for the effects of variations in calibration and instrument baselines, solar and solar system emissions, RFI, and data analysis errors. The quadrature sum of all systematic uncertainties in a typical map, after corrections, is less than 8.5 μK for rms sky fluctuations, less than 3 μK for the quadrupole and higher order multipole moments, and less than 30 μK^2 for the correlation function (all limits 95% CL). These limits represent a factor of 20 improvement over our previous upper limits (Smoot et al. 1991).

3. RESULTS

The DMR maps are dominated by two features: a dipole anisotropy and the emission from the Galactic plane. The dipole anisotropy ($\Delta T/T \approx 10^{-3}$) is seen consistently in all channels with a thermodynamic temperature amplitude 3.36 ± 0.1 mK in the direction $l = 264.7 \pm 0.8$, $b = 48.2 \pm 0.5$. Motion of an observer with respect to the CMB (a blackbody radiation field) produces a dipole anisotropy. We assume that the entire observed dipole results from our peculiar velocity and remove from the maps the dipole and the ≈ 1.3 μK–rms kinematic quadrupole produced by the second-order Doppler effect.

The corrected maps show no obvious features away from the Galactic plane. The 2°.6 pixel signal distribution roughly agrees with the expected instrument noise (≈ 150 μK). No 7° region varies from the mean by more than 210 μK ($\Delta T/T \approx 8 \times 10^{-5}$). Detection of additional features, other than receiver noise and the Galaxy, requires careful statistical analysis and/or averaging over larger angles.

3.1. *Structure in the Maps*

Figure 1 (Plates L1–L3) shows the 31, 53, and 90 GHz maps as smoothed with a Gaussian of 7° FWHM, which when convolved with the approximate 7° FWHM antenna beam, results in a 10° smoothing on the sky. The observed variance of the maps is the quadrature sum of the instrument noise and the intrinsic fluctuations on the sky:

$$\sigma^2_{\rm obs} = \sigma^2_{\rm DMR} + \sigma^2_{\rm sky} .$$

The two-channel (A + B)/2 sum maps provide an estimate of $\sigma^2_{\rm obs}$ and the channel (A − B)/2 difference maps provide an estimate of $\sigma^2_{\rm DMR}$ (Table 1) yielding $\sigma_{\rm sky}(10°) = 30 \pm 5$ μK for $|b| > 20°$.

TABLE 1

MAP RMS[a] AT 10° SMOOTHING FOR VARIOUS GALACTIC CUTS $|b| > x°$ IN MICROKELVINS

ν (GHz)	$\lvert b\rvert > x°$	$\sigma_{\rm obs}$ (A + B)/2	$\sigma_{\rm DMR}$ (A − B)/2	$\sigma_{\rm sky}(10°)$
31	10	133	94	95^{+6}_{-6}
31	20	101	96	33^{+9}_{-11}
31	30	97	95	20^{+21}_{-20}
31	40	101	96	30^{+12}_{-15}
53	10	55	36	41^{+4}_{-4}
53	20	46	35	30^{+4}_{-5}
53	30	47	36	30^{+5}_{-5}
53	40	47	36	30^{+5}_{-5}
90	10	69	59	35^{+6}_{-7}
90	20	65	61	22^{+7}_{-10}
90	30	67	60	29^{+7}_{-8}
90	40	67	59	31^{+7}_{-8}
RG	10	67	59	31^{+7}_{-9}
RG	20	65	59	27^{+7}_{-10}
RG	30	67	61	27^{+7}_{-10}
RG	40	68	62	28^{+7}_{-10}

[a] Uncertainties are 68% CL and include systematic effects.

All six channels show a statistically significant quadrupole signal. A comparison of the fitted quadrupoles between channels and frequencies, and between the first and second 6 months of data, shows that individual quadrupole components, Q_i, typically differ from map to map by ≈ 10 μK with comparable uncertainty. The χ^2 for 5 degrees of freedom ranged from one to 11 in various comparisons, corresponding to confidence levels ranging from 97% to 5% for agreement. Table 2 shows the frequency dependence of the quadrupole components. The large-scale Galactic emission away from the Galactic plane is predominantly quadrupolar. In Galactic coordinates, Q_1 aligns very well, although with opposite sign, with a cosecant ($|b|$) signal. Contamination by Galactic emission is evident from the systematic decrease of Q_1 with increasing Galactic latitude cut angle. Q_4 is the quadrupole component next most aligned with features of Galactic emission. Determination of the cosmic quadrupole is linked to its separation from Galactic emission (Bennett et al. 1992b). The best estimated cosmic signal has amplitude $Q_{\rm rms} = 13 \pm 4$ μK, corresponding to $\Delta T/T \approx 5 \times 10^{-6}$, which is more than 100 times smaller than the dipole.

The correlation function, $C(\alpha) = \langle T_1 T_2 \rangle$, which is the average product of temperatures separated by angle α, provides further evidence of the structure. $C(\alpha)$ is calculated for each map by rejecting all pixels with Galactic latitude $|b| < 20°$, removing the mean, dipole, and quadrupole from the remaining pixels, multiplying all possible pixel pair temperatures, and averaging the results into 2°.6 bins. Sample cross correlation functions shown in Figures 2 and 3 have a 2°.6 binning angle, 2°.6 map pixelization, a 1°.3 smearing due to the 0.5 s instrument sampling time and 3° rms DMR beam profile. When combined these produce an effective 3°.2 rms Gaussian smoothing. The observed correlation functions exhibit struc-

TABLE 2

QUADRUPOLE THERMODYNAMIC AMPLITUDE IN MICROKELVINS[a]

ν	b_{cut}	Q_{rms}	Q_1	Q_2	Q_3	Q_4	Q_5
31	10°	66 ± 8	-141 ± 16	27 ± 12	-4 ± 12	21 ± 14	12 ± 14
31	20	26 ± 9	-41 ± 20	10 ± 12	-6 ± 11	23 ± 17	19 ± 19
31	30	25 ± 13	-30 ± 25	3 ± 12	-4 ± 13	40 ± 25	4 ± 24
53	10	19 ± 3	-35 ± 6	19 ± 5	8 ± 4	1 ± 6	8 ± 5
53	20	11 ± 3	-9 ± 7	14 ± 5	8 ± 5	10 ± 7	3 ± 7
53	30	11 ± 4	3 ± 6	12 ± 6	8 ± 5	14 ± 8	3 ± 10
90	10	17 ± 4	-25 ± 9	16 ± 6	16 ± 5	9 ± 6	6 ± 8
90	20	14 ± 4	5 ± 8	12 ± 6	16 ± 5	16 ± 9	3 ± 7
90	30	15 ± 5	13 ± 10	11 ± 6	18 ± 5	17 ± 14	4 ± 9
RG.....	10	13 ± 4	11 ± 9	16 ± 8	15 ± 9	-2 ± 9	4 ± 8
RG.....	20	13 ± 5	11 ± 10	16 ± 8	16 ± 10	8 ± 10	-3 ± 9
RG.....	30	15 ± 6	18 ± 13	16 ± 9	18 ± 12	6 ± 12	3 ± 14

[a] Uncertainties are 68% CL and include systematic effects. The Q_i are the peak values for each component of the quadrupole, $Q(l, b)$. $Q(l, b) = Q_1(3 \sin^2 b - 1)/2 + Q_2 \sin 2b \cos l + Q_3 \sin 2b \sin l + Q_5 \cos^2 b \sin 2l$. $Q^2_{rms} = 4/15[(3/4)Q_1^2 + Q_2^2 + Q_3^2 + Q_4^2 + Q_5^2)]$. The Q_i are corrected for the Doppler effect which is aligned with the dipole and have amplitudes of $\sim 2\ \mu$K.

ture on all scales from the beam size (7°) to the quadrupole (90°) and differ significantly ($> 7\ \sigma$) from the flat correlation function due to receiver noise alone, e.g., the (A − B)/2 maps correlation function.

3.2. *Galactic Emission*

The chosen observing frequencies give an optimal and large ratio between CMB and Galactic emission. Nevertheless, at these sensitivities Galactic emission is a significant concern and must be understood before one can make cosmological interpretations (Bennett et al. 1992b). A summary of the Galactic emission contribution follows.

Galactic emission antenna temperature is dominated by three components: synchrotron emission $\propto \nu^{-2.75}$, free-free emission $\propto \nu^{-2.1}$ and dust emission $\propto \nu^{1.5}$, as shown in Figure 1 of Bennett et al. (1992b). The detected signals expressed in thermodynamic temperature are nearly constant amplitude: 10° sky–rms $\propto \nu^{-0.3 \pm 1}$ and quadrupole and correlation function $\propto \nu^{-0.2 \pm 1}$. The flat spectral index of our results, without correction for Galactic emissions, is consistent with a cosmic origin and inconsistent with an origin from a single Galactic component. While we cannot rule out a correlated superposition of dust, synchrotron, and free-free emission, it would require significantly different spatial distributions at high Galactic latitudes than previously known. Bennett et al. (1992b) find this unlikely.

The correlation function (Fig. 2) and rms sky fluctuation (Table 1) are independent of Galactic latitude cut angle after excluding the Galactic plane region. The results are affected significantly when the $|b| < 10°$ region is included, but are

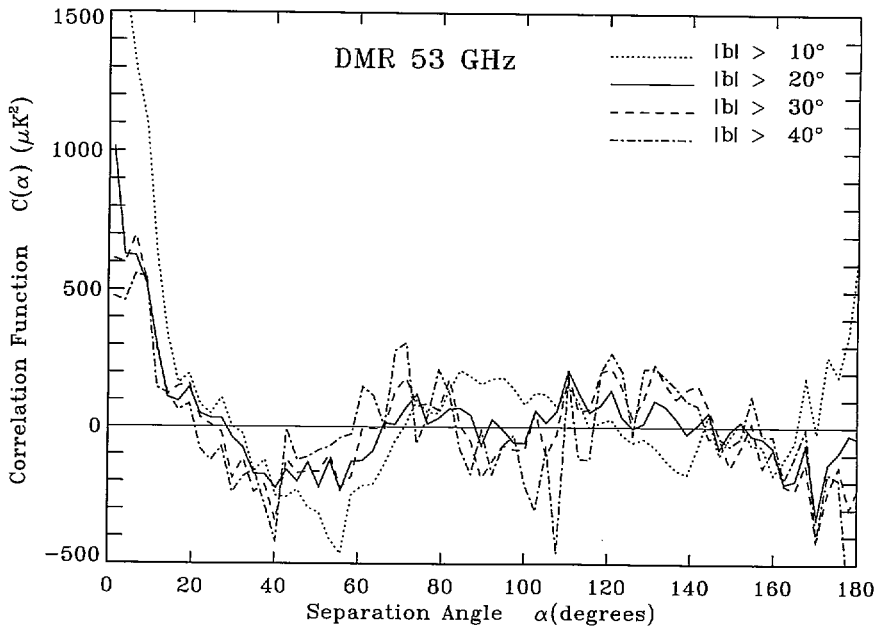

FIG. 2.—Correlation functions, $C(\alpha)$, at various Galactic latitude cuts for the 53 GHz map with mean, dipole, and quadrupole removed, demonstrating near independence of Galactic latitude cuts beyond $|b| > 20°$.

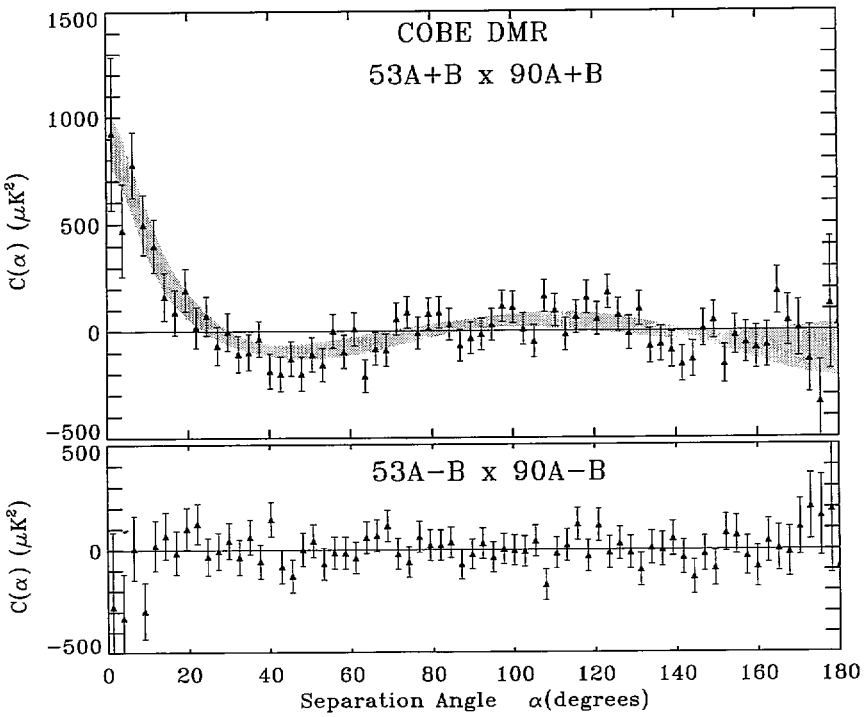

FIG. 3.—Cross-correlation of 53 GHz with 90 GHz for $|b| > 20°$ plus the correlation function for a scale-invariant spectrum with an expected quadrupole amplitude of 15.4 μK: the gray band indicates 68% C.L. cosmic variations. *Top* is for the sum maps, and *bottom* is for the difference maps. The cross and autocorrelations for the various combination of maps all have consistent values.

stable for cuts $|b| > 15°$ for 53 and 90 GHz. The 31.5 GHz data show measurable effects to $|b| \approx 30°$. Cross-correlations for $|b| > 20°$ of the 19 GHz map (Boughn et al. 1992) with the 53A + B map and of the FIRAS dust map (Wright et al. 1991) with the 90A + B map indicate that scaling of Galactic signals would account for $\sim 10\%$ of the structure in the maps. Removing the estimated Galactic emission causes no significant change in our results for $|b| > 20°$, as expected from the cross-correlation results.

Since Galactic emission is weak at high latitudes, for statistic analysis we construct a map from the six DMR channels designed to compromise between significantly Reduced Galactic (RG) emission and minimum noise:

$$\text{RG map} = -0.440 \times 31 \text{ GHz map} + 1.030 \times 53 \text{ GHz map} + 0.564 \times 90 \text{ GHz map} .$$

The resultant map is in units of Planck brightness temperature and has residual free-free and synchrotron emission well below the observed structure for $|b| > 20°$. The fitted dipole amplitude and direction is essentially identical to the weighted average of all the channels. The rms sky variation, quadrupole, and correlation functions for the "Reduced Galaxy" map are consistent with those from the 53 and 90 GHz maps for the Galactic latitude cuts $|b| > 20°$ (Tables 1 and 2).

4. DISCUSSION

The *COBE* DMR maps show structure with characteristic anisotropy of $\Delta T/T \approx 6 \times 10^{-6}$. The structure is larger and of a different character than all identified systematic errors. A critical issue is whether the structure is due to Galactic or extragalactic emissions or is in the cosmic microwave background. Although one cannot rule out a heretofore undiscovered Galactic or extragalactic emission, the Galactic or discrete extragalactic origin of the measured anisotropy would require an unlikely confluence of factors. It would require the source of anisotropy to mimic a thermal spectrum and, if Galactic, not have the spatial distribution associated with known components of the Galaxy. Discrete extragalactic sources individually contribute less than 2 μK in the DMR beam and the expected temperature variations are less than 1 μK (Franceschini et al. 1989). The most economical hypothesis is to attribute the structure to the microwave background.

Interpreted as CMB anisotropy, these results test inflationary models of cosmology (Guth 1981; Linde 1982; Albrecht & Steinhardt 1982), which predict a nearly scale-invariant spectrum of density perturbations (Bardeen, Steinhardt, & Turner 1983; Guth & Pi 1982; Hawking 1982; Starobinskii 1982). They also test gravitational instability models of structure formation (e.g., Bond & Efstathiou 1987; Holtzman 1989). The measured correlation function determines the parameters of the fluctuation power spectrum. A power-law primordial density fluctuation spectrum of the form $P(k) = Ak^n$ is equivalent to a CMB temperature anisotropy spectrum for the rms difference in temperatures separated by angle θ of the approximate form $\Delta T_{\rm rms} \propto \theta^{(1-n)/2}$. The scale-invariant value $n = 1$ gives a CMB temperature fluctuation spectrum that is approximately independent of the separation angle for angles larger than the beam size. The correlation function is

$$C(\alpha) = \sum_{l>2} \Delta T_l^2 \, W(l)^2 P_l[\cos(\alpha)] ,$$

where a 3°2 rms Gaussian beam gives a weighting $W(l) = \exp\{-1/2[l(l+1)/17.8^2]\}$ and

$$\Delta T_l^2 = \frac{1}{4\pi}\sum_m |a_{lm}|^2$$

are the rotationally invariant rms multipole moments. The predicted moments, as a function of spectral index n, are given by (Bond & Efstathiou 1987; we adjust the formula for the correlation function variance by a factor of 2):

$$\langle \Delta T_l^2 \rangle = (Q_{\rm rms-PS})^2 \frac{(2l+1)}{5}\frac{\Gamma[l+(n-1)/2]\Gamma[(9-n)/2]}{\Gamma[l+(5-n)/2]\Gamma[(3+n)/2]}.$$

$Q_{\rm rms-PS}$ is the $Q_{\rm rms}$ predicted by the measured higher order moments of the power spectrum when a power law is assumed. The best-fitted values correspond to $n = 1.1 \pm 0.5$ and $Q_{\rm rms-PS} = 16 \pm 4\ \mu$K. Forcing the spectral index to $n = 1$ gives $Q_{\rm rms-PS} = 16.7 \pm 4\ \mu$K and increases the χ^2 from 79 to 81 for 68 degrees of freedom.

If the observed structures result from a power-law spectrum of primordial fluctuations with a Gaussian distribution, the ΔT_l^2 in each horizon have a χ^2 distribution of $2l+1$ degrees of freedom, giving a cosmic variance of $2\langle \Delta T_l^2\rangle^2/(2l+1)$. Including the cosmic variance results in best-fitted values $n = 1.15^{+0.45}_{-0.65}$ and $Q_{\rm rms-PS} = 16.3 \pm 4.6\ \mu$K with a χ^2 of 53. Figure 3 shows the cross-correlation of the 53 and 90 GHz maps, along with the predicted shape for the best-fitted scale-invariant spectrum. Including cosmic variance, our data are consistent with power-law spectra in the range $n = 1 \pm 0.6$ and $Q_{\rm rms-PS} = 17 \pm 5\ \mu$K.

The observed cosmic quadrupole ($Q_{\rm rms} = 13 \pm 4\ \mu$K) is slightly below the mean value predicted by the higher order moments ($Q_{\rm rms-PS} = 16 \pm 4\ \mu$K). This is a likely consequence of cosmic variance: the mode of the χ^2 distribution is lower than the mean. A quadrupole value of 13 μK or lower would be expected to occur 35% of the time. The observed quadrupole has some uncertainty in its corrections for Galactic emissions, the Doppler shift, and its particular systematic errors (e.g., a pointing error can modulate the dipole anisotropy into a small quadrupole). The results above exclude the quadrupole from the maps before computing $C(\alpha)$. Including the quadrupole increases n and the χ^2 and decreases $Q_{\rm rms-PS}$ to typical values of $n = 1.5$ and $Q_{\rm rms-PS} = 14\ \mu$K.

The measured parameters—the rms fluctuations on a 10° scale, $\sigma_{\rm sky}(10°)$, the rms quadrupole amplitude, $Q_{\rm rms}$, and the correlation function and its derivatives: the spectral index, n, and quadrupole-normalized power-law amplitude, $Q_{\rm rms-PS}$—are consistent with a Harrison-Zel'dovich (scale-invariant) spectrum of perturbations, which predicts $Q_{\rm rms} = (1^{+0.3}_{-0.4})Q_{\rm rms-PS}$ and $\sigma_{\rm sky}(10°) = (2.0 \pm 0.2)Q_{\rm rms-PS}$. The theoretical 68% CL errors take into account the cosmic variance due to the statistical fluctuations in perturbations for our observable portion of the universe. The minimum $Q_{\rm rms}$ for models with an initial Harrison-Zel'dovich perturbations, normalized to the local large-scale galaxy streaming velocities, is predicted to be 12 μK, independent of the Hubble constant and the nature of dark matter (Gorski 1991; Schaefer 1991).

These observations are consistent with inflationary cosmology models. The natural interpretation of the DMR signal is the observation of very large (presently $\gg 100$ Mpc) structures in the universe which are little changed from their primordial state ($t \ll 1$ s). These structures are part of a power-law spectrum of small amplitude gravitational potential fluctuations which on smaller length scales are sources of the large-scale structure in the universe as observed today. The accompanying paper by Wright et al. (1992) interprets the DMR data's constraints on gravitational instability theories.

The *COBE* DMR instrument continues to operate well and has completed its second year of observations. New data and continuing analysis are expected to improve our sensitivity to structure in the maps. If this structure is CMB anisotropy and the spectrum is scale free, then several experiments are within a factor of 2 of detecting anisotropy and a new branch of astronomy has commenced.

The *COBE* DMR results originate in the excellent work by the staff of the *COBE* Project and the support of the Office of Space Sciences and Applications of NASA Headquarters. We thank those engineers and others who helped design and build the DMR instrument and operate the satellite. We also thank the data analysts who provided the attitude and other spacecraft information, including A. Banday, V. Kumar, R. Kummerer, and J. Santana.

REFERENCES

Albrecht, A., & Steinhardt, P. J. 1982, Phys. Rev. Lett., 48, 1220
Bardeen, J. M., Steinhardt, P. J., & Turner, M. S. 1983, Phys. Rev. D, 28, 679
Bennett, C. L., et al. 1992a, ApJ, 391, 466
———. 1992b, ApJ, 396, L7
Bond, J. R., & Efstathiou, J. 1987, MNRAS, 226, 655
Boggess, N., et al. 1992, ApJ, in press
Boughn, S. P., Cheng, E. S., Cottingham, D. A., & Fixsen, D. J. 1992, ApJ, 391, L49
Fixsen, D. J., Cheng, E. S., & Wilkinson, D. T. 1983, Phys. Rev. Lett., 50, 620
Franceschini, A., Toffolatti, L., Danese, L., & De Zotti, G. 1989, ApJ, 344, 35
Gorski, K. 1991, ApJ, 370, L5
Guth, A. 1981, Phys. Rev. D, 23, 347
Guth, A., & Pi, Y.-S. 1982, Phys. Rev. D, 1110
Haslam, C. G. T., et al. 1981, A&A, 100, 209
Hawking, S. 1982, Phys. Lett., 115B, 295
Holtzman, J. A. 1989, ApJS, 71, 1
Janssen, M. A., & Gulkis, S. 1992, in The Infrared and Submillimeter Sky after *COBE*, ed. M. Signore & C. Dupraz (Dordrecht: Kluwer)
Klypin, A. A., Sazhin, M. V., Strukov, I. A., & Skulachev, D. P. 1987, Soviet Astron. Lett., 13, 104
Kogut, A., et al. 1992, ApJ, in press
Linde, A. 1991, Phys. Lett., 108B, 389
Lubin, P., Villela, T., Epstein, G., & Smoot, G. 1985, ApJ, 298, L1
Meyer, S. S., Page, L., & Cheng, E. S. 1991, ApJ, 371, L7
Sachs, R. K., & Wolfe, A. M. 1967, ApJ, 147, 73
Schaefer, R. K. 1991, in AIP Conf. Proc. 222, After the First Three Minutes, ed. S. S. Holt, C. L. Bennett, & V. L. Trimble (New York: AIP), 119
Smoot, G., et al. 1990, ApJ, 360, 685
———. 1991, ApJ, 371, L1
Starobinskii, A. A. 1982, Phys. Lett., 117B, 175
Torres, S., et al. 1989, Data Analysis in Astronomy 1988, ed. V. di Gesu, L. Scarsi, & M. C. Maccarone (New York: Plenum), 319
Wright, E. L., et al. 1991, ApJ, 381, 200
Wright, E. L., et al. 1992, ApJ, 396, L13

1992ApJ...396L...1S

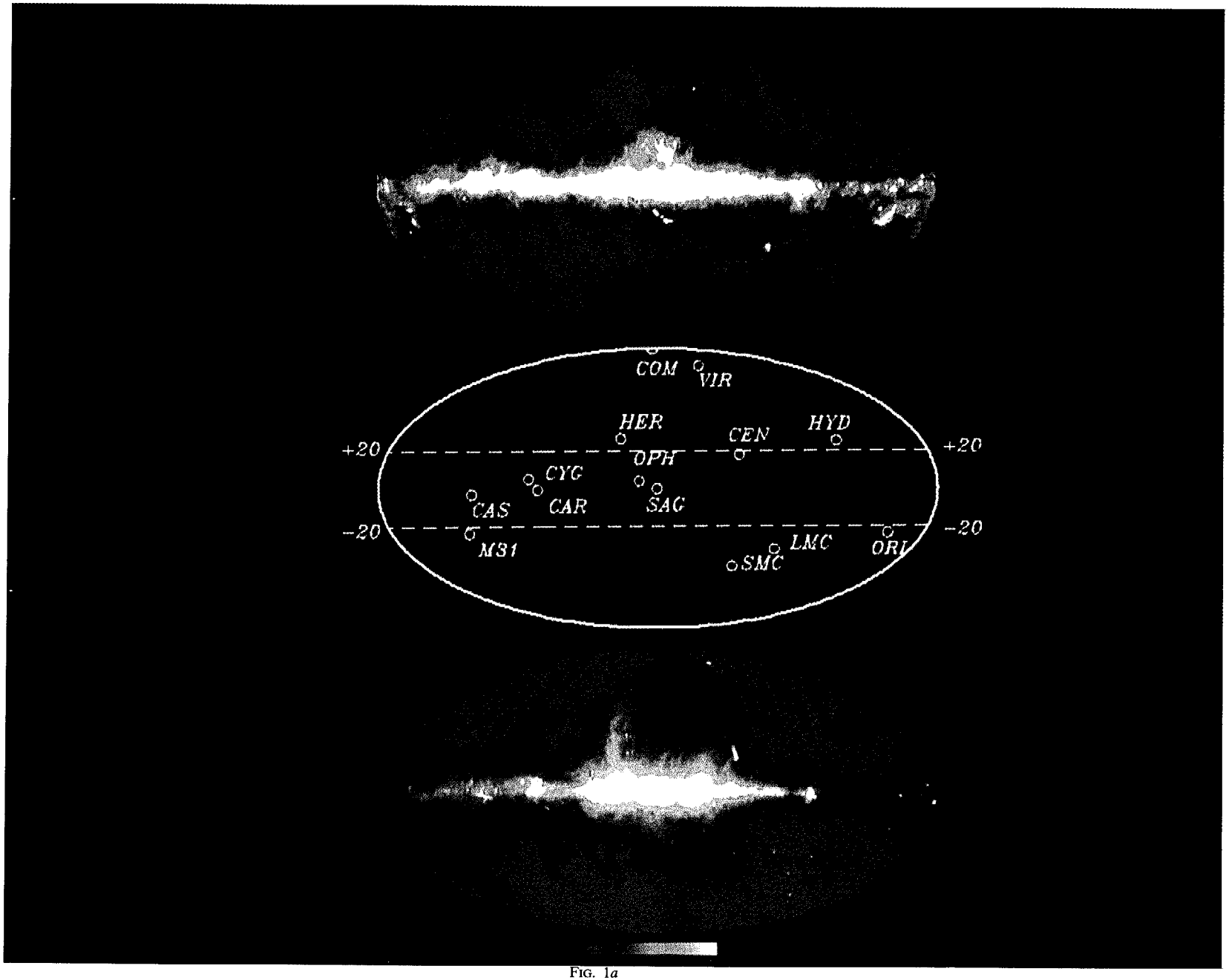

FIG. 1*a*

FIG. 1.—(*a*) Maps and overlay for comparison with *COBE* DMR maps: *Top*, *IRAS* 100 μm zodi-removed dust map. *Middle*, Galactic coordinate grid and source positions. *Bottom*, the Haslam et al. 408 MHz sky survey. (*b*) *COBE* DMR (A + B)/2 maps at 31, 53, and 90 GHz. The maps have been smoothed with a 7° FWHM Gaussian, which when combined with the approximately 7° FWHM Gaussian beam shape results in about a 10° smoothing on the sky. (*c*) *COBE* DMR (A − B)/2 maps at 31, 53, and 90 GHz. The maps are processed identically as (*b*). The sky signal is canceled by the subtraction but the average instrument noise remains the same.

SMOOT et al. (see 396, L2)

PLATE L1

1992ApJ...396L...1S

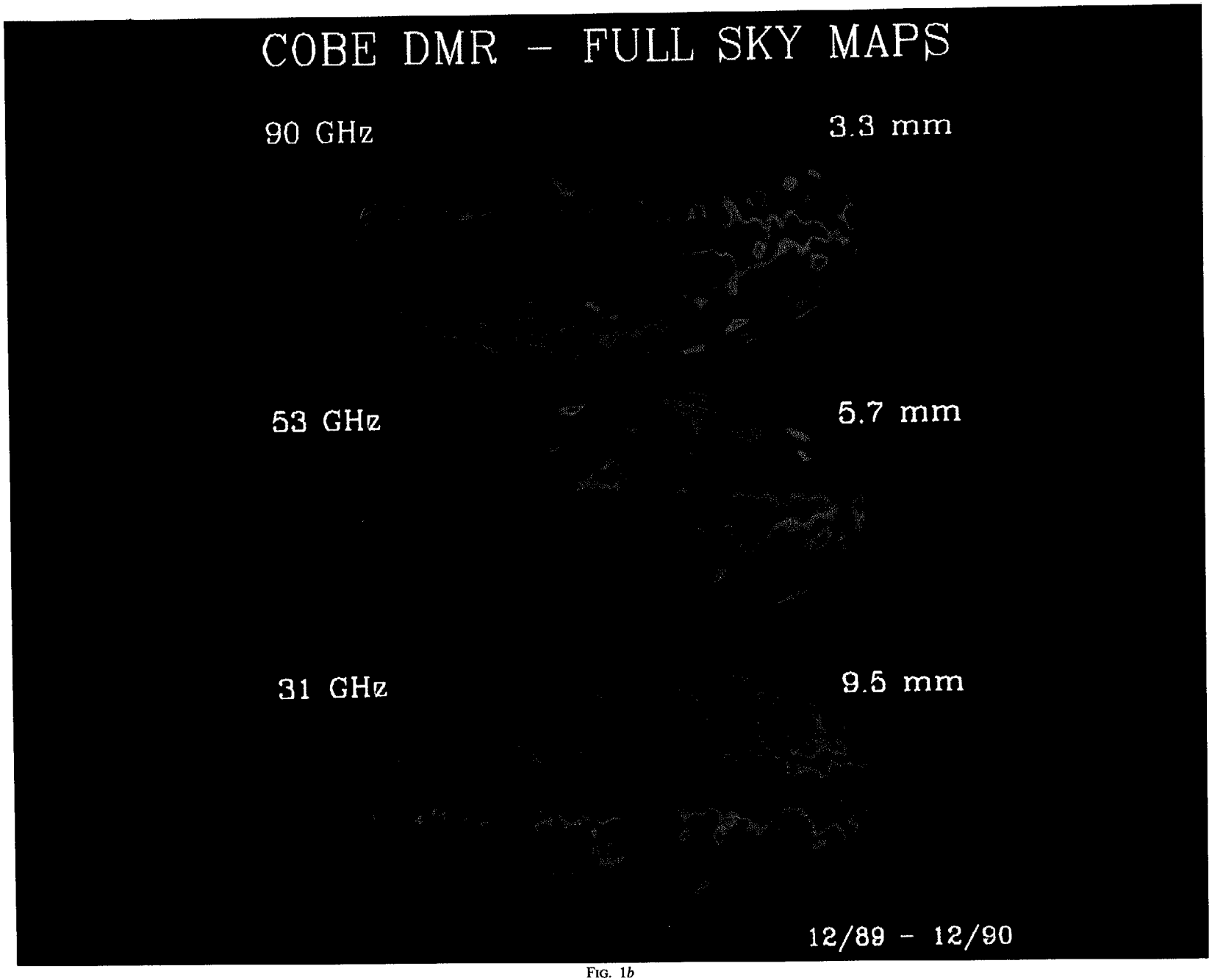

FIG. 1*b*

SMOOT et al. (see 396, L2)

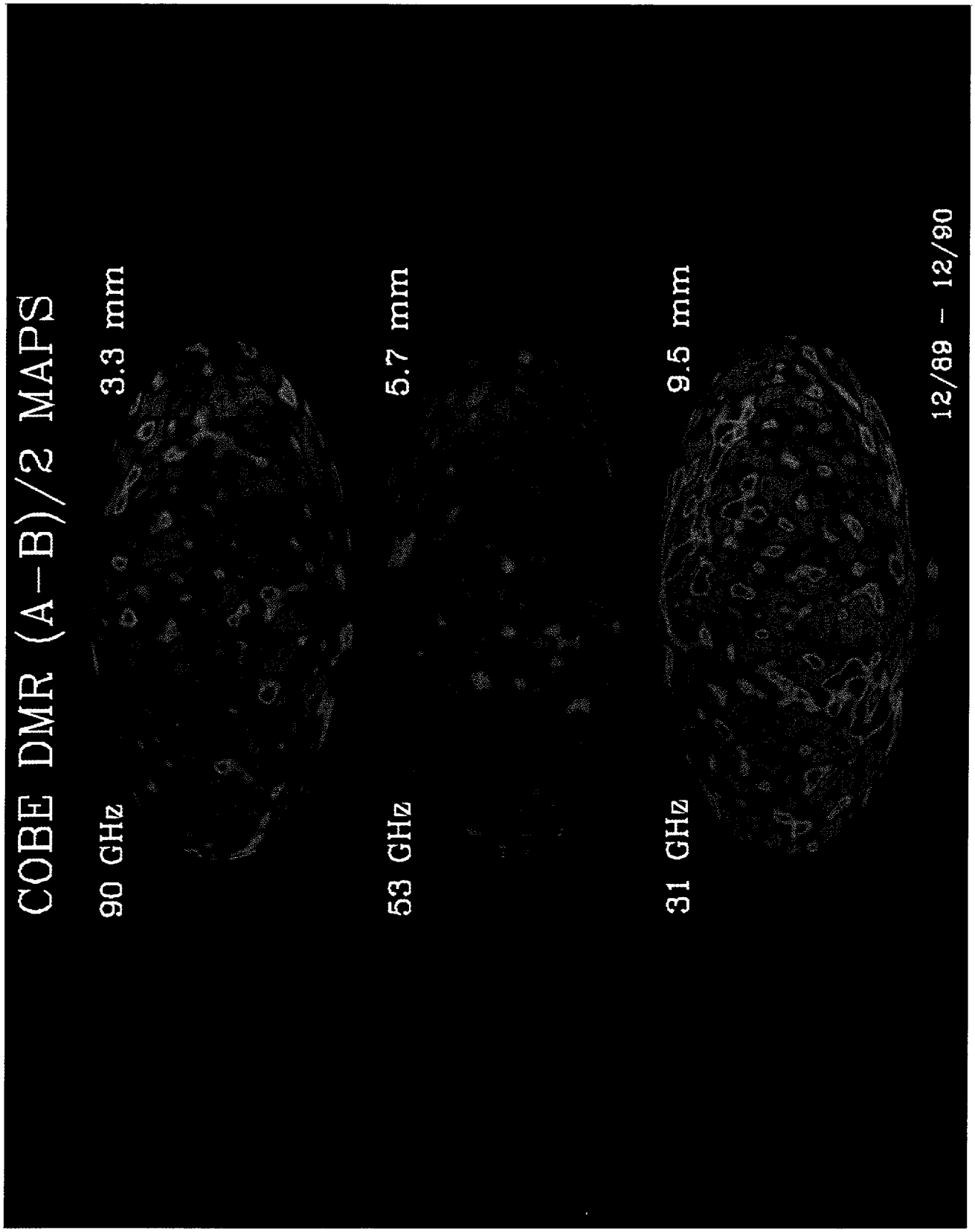

FIG. 1*c*

SMOOT et al. (see 396, L2)